ACS APPLIED MATERIALS & INTERFACES

Research Article

www.acsami.org

The Effect of Treatment Temperature on Corrosion Resistance and Hydrophilicity of an Ionic Liquid Coating for Mg-Based Stents

Yafei Zhang,[†,‡] Maria Forsyth,*[,†,‡] and Bruce R. W. Hinton[†]

[†]Institute for Frontier Materials, Deakin University, Burwood, Victoria 3125, Australia

[‡]Australian Research Council Centre of Excellence for Electromaterials Science, Deakin University, Burwood, Victoria 3125, Australia

ABSTRACT: Mg alloys are attractive candidate materials for biodegradable stents. However, there are few commercially available Mg-based stents in clinical use because Mg alloys generally undergo rapid localized corrosion in the body. In this study, we report a new surface coating for Mg alloy AZ31 based on a low-toxicity ionic liquid (IL), tributyl(methyl)-phosphonium diphenyl phosphate ($P_{1,4,4,4}$dpp), to control its corrosion rate. Emphasis is placed on the effect of treatment temperature. We showed that enhancing the treatment temperature provided remarkable improvements in the performances of both corrosion resistance and biocompatibility. Increasing treatment temperature resulted in a thicker (although still nanometer scale) and more homogeneous IL film on the surface. Scanning electron microscopy and optical profilometry observations showed that there were many large, deep pits formed on the surface of bare AZ31 after 2 h of immersion in simulated body fluid (SBF). The IL coating (particularly when formed at 100 °C for 1 h) significantly suppressed the formation of these pits on the surface, making corrosion occur more uniformly. The $P_{1,4,4,4}$dpp IL film formed at 100 °C was more hydrophilic than the bare AZ31 surface, which was believed to be beneficial for avoiding the deposition of the proteins and cells on the surface and therefore improving the biocompatibility of AZ31 in blood. The interaction mechanism between this IL and AZ31 was also investigated using ATR-FTIR, which showed that both anion and cation of this IL were present in the film, and there was a chemical interaction between dpp^- anion and the surface of AZ31 during the film formation.

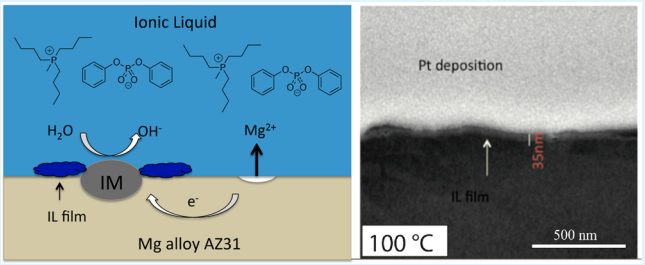

KEYWORDS: *biodegradable stents, Mg alloy, ionic liquid, corrosion protection, morphology, hydrophilic surface*

1. INTRODUCTION

Coronary heart disease is more common than what we think. It is one of the leading causes of death all over the world. Implanting stents into diseased vessels is considered as an effective treatment for heart disease.[1] In practice, biodegradable stents are preferable to permanent stents, as they can provide temporary opening of narrowed arteries and be gradually dissolved sometime after the arteries have recovered, which can effectively avoid the side effects due to the long-term presence of permanent stents in the vessels.[2] Recently, the study of degradable stents has become an important issue in the field of biomaterial implants. Mg alloys are of interest as candidates for biodegradable stents materials, owing to their (1) well-known biocompatibility and (2) degradability in the body, so that the Mg stents can be consumed and bioabsorbed in the body. Furthermore, these alloys have excellent mechanical properties: the strength level of Mg alloys can be up to 330 MPa, which is high enough to maintain the opening of a coronary artery.[2−4]

The main limitation to the application of Mg alloys as a material for stents is their fast corrosion rate. Side effects of fast corrosion include the generation of a large amount of hydrogen bubbles in the vessel in a short period and high local pH increase that can damage the surrounding tissues.[5] Besides, the corrosion morphology of Mg alloys is localized and nonuniform due to the galvanic potential difference between the Mg matrix and intermetallic particles in the microstructure.[6] This localized corrosion morphology can lead to the early loss of mechanical integrity and thus premature failure before the stent "fixes" the problem.[7] Moreover, another concern involves interactions occurring at the interface of the stent with the surrounding tissue, which leads to the accumulation of proteins from the blood and the cell proliferation on a bare metallic coronary stent and thereby the in-stent restenosis and the formation of thrombosis.[8,9]

Many efforts have been devoted to prolonging the degradation time and increase the biocompatibility of Mg alloys. A typical method is the formation of a biocompatible and corrosion protective surface coating. Chromate conversion coating, although commercially used as a means of providing some corrosion protection for Mg alloys, is not appropriate for biomedical applications, as leaching of chromate from the coating can take place, which is carcinogenic.[10] Over recent decades, alternative chromate-free coatings have been subjected to intensive study, including surface modification via anodizing,[11] the use of alternative conversion coatings (e.g., calcium phosphate coating, silane based coatings[12]), and organic

Received: July 23, 2014
Accepted: October 15, 2014
Published: October 15, 2014

deposited polymeric coatings (e.g., polylactic-*co*-glycolic coating[13]). Each of these coating systems has merits and limitations. Most coatings for Mg alloys described in the literature have not been advanced for clinical applications, and no commercial products are available in the biomedical devices sector. Therefore, there is need for research into finding a solution to the problem of Mg alloy corrosion.

Recently, the use of ionic liquid (IL) films for environmentally friendly organic-based coatings has increasingly attracted interest for the corrosion protection of Mg alloys. ILs are low-temperature molten salts and have a melting point below 100 °C.[14] One advantage of using ILs for forming a surface coating on a metallic substrate is the unique property of having a high concentration of reactive species compared with solutions. In addition, ILs are "designable" materials in the sense that combinations of desired properties can be achieved by altering the chemical structures of the cation and anion pair, for example, introducing functional amine groups into the ions for drug delivery purpose.[15] In the life sciences, ILs also have shown unexpected opportunities. For example, ILs have been highlighted for their potential use as pharmaceuticals[16] and antimicrobials.[17] Furthermore, ILs can act as protein-stabilizing agents[18] and be solvents for enzymes.[19]

Therefore, control over the corrosion rate and surface biocompatibility of Mg alloys is likely to be achieved by developing a specific IL surface coating. Two phosphate-based ionic liquids (trihexyl(tetradecyl)phosphonium diphenylphosphate ($P_{6,6,6,14}$dpp)[20] and trihexyl(tetradecyl)phosphonium bis(2,4,4-trimethyl-pentyl)phosphinate ($[P_{6,6,6,14}][(^iC8)_2PO_2]$)[21] have been investigated for the corrosion protection for a number of Mg alloys, which was mainly motivated by the reactivity of phosphate with magnesium. Both of them exhibited good corrosion protection ability for Mg alloys. However, these ionic liquids are not likely to be biocompatible due to the long hydro-carbon (H−C) chains on the cation, which can be lipophilic and can disrupt the membrane of cells, causing death of the cells.[17] The importance of surface activation by either increased treatment temperature[21] or applied bias potential[22] was also suggested in the prior work for the treatment with the trihexyl(tetradecyl)-phosphonium bis(2,4,4-trimethyl-pentyl)phosphinate $[P_{6,6,6,14}][(^iC8)_2PO_2]$ IL on an AZ31 Mg alloy; however, a systematic investigation of the effect of these parameters on the IL surface film structure and influence on corrosion morphology has not yet been undertaken. Previous work has also indicated that both anion and cation components of the IL existed in the IL film, and thus, the effect of changing the cation is also of interest.

We have carefully selected and synthesized an IL tributyl-(methyl)phosphonium diphenylphosphate ($P_{1,4,4,4}$dpp), which contains short hydrocarbon (H−C) chains in the cation and is therefore believed to increase the hydrophilicity and thus its biocompatibility with surrounding tissues. In a previous study, a cytotoxic test was conducted on $P_{1,4,4,4}$dpp, and its toxicity was considered acceptable for coronary artery cells.[20] It was also demonstrated that this IL was able to react with the AZ31 surface to provide a certain level of corrosion protection for the Mg alloy AZ31 in simulated body fluid (SBF); however, in that work, the IL film was not robust, and excessive corrosion still occurred on the IL-treated sample surface.[20] Thus, there is still a need to improve the effectiveness of the $P_{1,4,4,4}$dpp coating in terms of both corrosion protection and biocompatibility.

In this work, emphasis is placed on investigating if increasing treatment temperature can form a more robust surface film. The effect of different treatment temperatures on the formation of the IL film on the AZ31 surface, and its corrosion performance has been investigated in detail. In literature, generally for related research, a SBF electrolyte is used to investigate the corrosion properties for such systems.[23−25] While the addition of protein and other biological compounds are likely to have an impact on corrosion and are sometimes incorporated into the testing electrolyte, the effect of protein absorption on the surface of an electrode is not clear yet. It has, in fact, been confirmed that protein absorption on the electrode surface will restrain the corrosion rate of metals.[26,27] Therefore, to simplify the analysis of the data and more clearly elucidate subtle differences between treatments, we have chosen SBF as the test medium in this work. The results indicate that, under an optimum temperature, a thin and homogeneous film can form on AZ31, which not only provides a reduced rate of corrosion but also modifies the corrosion morphology to mitigate dangerous localized corrosion and increases the surface hydrophilicity. In addition, the interaction mechanisms underlying the formation of the IL film on AZ31 surface are also investigated. These studies are believed to be important steps toward the application of this IL coating for biodegradable Mg-based stents.

2. EXPERIMENTAL SECTION

2.1. Samples and Solutions. The substrate investigated was a direct strip cast Mg alloy AZ31. While this alloy contains aluminum, it has been suggested that the AZ31 alloy, contains a tolerable level of aluminum believed to be acceptable for use in the human body.[28] Samples (5 × 5 × 5 mm) were epoxy mounted, ground with SiC paper to a 4000-mesh finish under running distilled water, and subsequently dried with nitrogen gas. Before each test, the sample was put into a vacuum desiccator for 1 h to stabilize the native passive MgO/$Mg(OH)_2$ film.

A SBF with similar ionic composition to that of human blood plasma was chosen as the test solution. It contained 103 mM Cl^-, 147 mM Na^+, 2.6 mM Ca^{2+}, 1.5 mM Mg^{2+}, 5 mM K^+, 6 mM HCO_3^-, 0.5 mM SO_4^{2-}, and 1 mM HPO_4^{2-}. The pH of the SBF was 7.4 ± 0.5, which was maintained with HEPES buffer (2-[4-(2-hydroxyethyl)-1-piperazin-1-yl] ethanesulfonic acid (Ajax Finechem) at a concentration of 17.892 g/L.

2.2. Synthesis of $P_{1,4,4,4}$dpp IL and IL Treatments on Mg Alloys. Tributyl(methyl)phosphonium diphenylphosphate ($P_{1,4,4,4}$dpp; Figure 1) was synthesized by the reaction of diphenyl phosphoric acid (Aldrich, Australia) with tributyl(methyl)-phosphonium methyl carbonate (CYPHOS IL 340). The synthesis route of this IL is shown in eq 1. The synthesized IL was then passed through a column containing a filter agent, alumina, and sand to remove any impurities and then dried under vacuum.

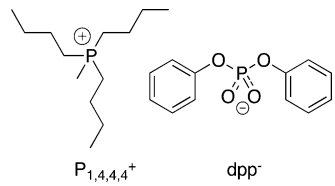

Figure 1. Chemical structures of the tributyl(methyl)phosphonium cation ($P_{1,4,4,4}^+$) and diphenylphosphate anion (dpp^-).

Synthesis route of ionic liquid tributyl(methyl)phosphonium diphenyl phosphate ($P_{1,4,4,4}$dpp).

$$P_{1,4,4,4}CH_3OCO_2 + Hdpp = P_{1,4,4,4}dpp + CH_3OH + CO_2\uparrow \quad (1)$$

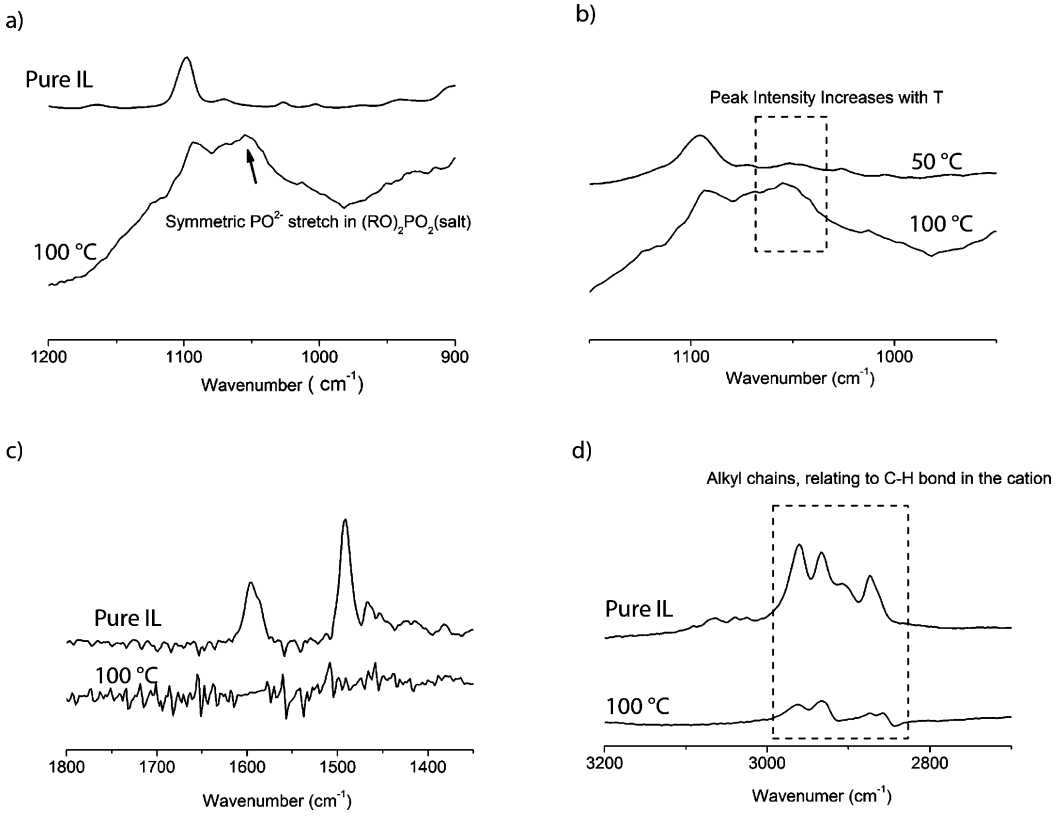

Figure 2. ATR-FTIR spectra of pure $P_{1,4,4,4}$dpp IL (containing approximately 300 ppm water) and surface of AZ31 treated with this IL at 100 °C for 1 h: (a) expansion of the range 1200−900 cm^{-1}, (b) comparison of ATR-FTIR spectra in the range of 1150−950 cm^{-1} for selected IL-treated samples treated at 50 and 100 °C, (c) expansion of the range 1800−1350 cm^{-1}, and (d) expansion of the range 3200−2700 cm^{-1}.

For the IL treatment, a plastic pipet was clamped to the epoxy-mounted sample to allow 0.15 mL of IL to be applied to the entire 5 × 5 mm area of the sample. This pipet arrangement was then placed in an oven to adjust the treatment temperature. Several different treatment temperatures were tested in this work: room temperature (RT) and 50, 65, 75, and 100 °C. The treatment time was typically 1 h in this work. After IL treatment, the surfaces of the AZ31 samples were thoroughly cleaned using ethanol and distilled water.

2.3. Characterization of IL Films. Attenuated total reflectance sampling used with Fourier transform infrared spectroscopy (ATR-FTIR) was performed on a Varian 3100 Excalibur series spectrometer using Varian Resolutions Pro Version 4.1 software. Scans (at 10 kHz with a resolution of 4 cm^{-1} and a sensitivity of 8) were performed on pure $P_{1,4,4,4}$dpp IL that contained approximately 300 ppm of water and, for comparison, on selected samples IL treated at 50 and 100 °C.

The thicknesses of the IL films formed after the 50 and 100 °C IL treatments were characterized using a FEI Quanta 3D FEG FIB-SEM instrument. Gallium ions were used to section the surface with a 5 nA current and to clean the edge of the cross section with 3 and 1 nA currents. A platinum (Pt) layer was deposited onto the surface prior to milling to protect the edge of the milled section. The cross section was then imaged using secondary electron SEM at an accelerating voltage of 5 kV.

Contact angle measurements were carried out on bare AZ31 and AZ31 samples IL treated at 50 and 100 °C using a Kruss DSA 100 (Hamburg, Germany) contact angle goniometer. Drops of Milli-Q water (5 μL) were placed on the surfaces, and the resulting image was captured and analyzed using the proprietary drop-shape analysis software. At least five angle measurements were obtained per sample, which were used to determine the mean angle ± standard deviation (SD).

2.4. Immersion Corrosion Testing. Bare and IL-treated AZ31 samples were immersed into 100 mL SBF at 37 °C. As Mg alloys corrode readily in aqueous solutions, a short exposure time of 2 h was sufficient for differences between samples to become apparent. The corrosion morphologies of these samples were then examined using a Philips XL20 scanning electron microscope with an accelerating voltage of 10 keV. The corrosion products were removed by immersion for 1 min in a solution of 200 g of chromium trioxide, 10 g of silver nitrate, and 20 g of barium nitrate in 1 L of distilled water at RT.

After removal of the corrosion product, the samples were analyzed using a Veeco Contour GT-K1 optical profilometer, which counted the pit numbers for each pit depth over a 937.5 × 1250 μm area. Mass loss analysis is commonly used to assess corrosion rate from such immersion tests. However, this is a bulk technique, which is not useful with respect to understanding the mechanisms of corrosion. Indeed, for localized corrosion, even if bulk mass loss is low, it is still a problem for a component or implant. Another difficulty with using mass loss for Mg is that removal of the surface layer is quite challenging, and the use of chromate solutions is necessary. The difficulty in completely removing surface products that may affect the accuracy of weight measurements also leads to uncertainty and error in the final results. Therefore, in this work, profilometry is used to ascertain corrosion damage and morphology because it is a much more sensitive surface technique. Furthermore, optical profilometry provides much greater accuracy of pit distribution and depth compared with cross sectioning, as has been previously shown.[29,30]

All immersion tests were performed in triplicate. Four or more points on each sample were examined, and the pit numbers at each pit depth were expressed as a mean ± SD.

2.5. Electrochemical Impedance Spectroscopy (EIS) Testing. EIS measurements were performed in a modified plastic three-electrode cell containing 150 mL of SBF with a saturated calomel reference electrode and a titanium mesh counter electrode. Data were taken at 10 min intervals for approximately 2.5 h over a frequency range of 50 kHz to 50 mHz with eight points per decade using a 10

mV AC amplitude perturbation. Acquisition of EIS data began immediately when the samples were immersed in the solution.

The EIS measurements were performed using a Biologic VMP 3/Z and repeated in triplicate to indicate the reproducibility of results. The Z-fit program in EC-Lab software was used to fit an equivalent circuit to the EIS spectra.

3. RESULTS AND DISCUSSION

3.1. Characterization of $P_{1,4,4,4}$dpp IL Films. The FTIR spectra of the IL-treated AZ31 samples were compared with the spectrum of pure IL. Figure 2 shows the distinct differences between the FTIR spectra of $P_{1,4,4,4}$dpp IL and AZ31 IL treated at 100 °C. As shown in Figure 2a, a new peak at ~1080 cm^{-1} was identified in the spectrum for the AZ31 substrate IL treated at 100 °C compared with the pure IL. The peak in this position has previously been assigned to the symmetric stretch of PO_2^- in $(RO)_2PO_2^-$ (salt) (R=H or C−H).[31] The presence of this peak indicates the formation of an IL film on the surface and shows the existence of a metal ester $[Mg-O-PO_2]^-$ bond in this film. The peak intensity of this newly formed ester group increased with increasing treatment temperature (Figure 2b). Figure 2c displays another significant difference observed in the IR spectra. As shown in Figure 2, there were two peaks at approximately 1580 and 1470 cm^{-1} identified in the spectrum for pure IL, which were attributed to the aromatic C−H and C═C stretching from the phenyl group of the anion. As these two peaks were not observed in the spectrum of the IL treated substrate, this either reflected that the phenyl groups from the anion were not present in the film formed by IL treatment of the AZ31 sample surface or that these groups laid on the surface in such a way that the ATR-FTIR spectrum could not detect them. Prior ToF-SIMS experiments on related systems suggested the phenyl groups are in fact present on an IL-treated Mg alloy surface.[32] Comparison of IR spectra (Figure 2d) indicated that the C−H chains from the cation were essentially unaffected by the treatment process, suggesting that the cations may adsorb onto the surface via electrostatic interactions.

The thicknesses of these IL films were examined by focused ion beam scanning electron microscopy (FIB-SEM). Figure 3

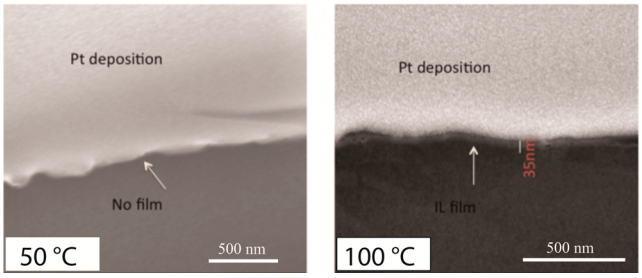

Figure 3. Comparison of cross sections of IL-treated AZ31 samples with treatment at (left) 50 °C and (right) 100 °C. These cross sections were obtained through ion-beam milling and observed by electron beam in the FIB-SEM.

shows cross sections of two IL films formed at 50 and 100 °C; note the clear evidence of the effect of treatment temperature on the thickness of IL film. In this figure, the light layer at the top of the image is a layer of Pt that was deposited within the FIB-SEM instrument. This Pt layer allows the identification of the thin surface film on the AZ31 surface. The IL film is visible as a distinct layer separating the Pt layer from the AZ31. As shown in Figure 3, there was no obvious IL film observed on the surface of the sample treated at 50 °C, possibly because that film was too thin to be seen. In contrast, when the treatment temperature was increased to 100 °C, a film about 35 nm thick could be observed sandwiched between the AZ31 substrate and the deposited layer of Pt.

The wettability of the sample surfaces was also determined, as shown in Figure 4. The surface of bare AZ31 had a contact

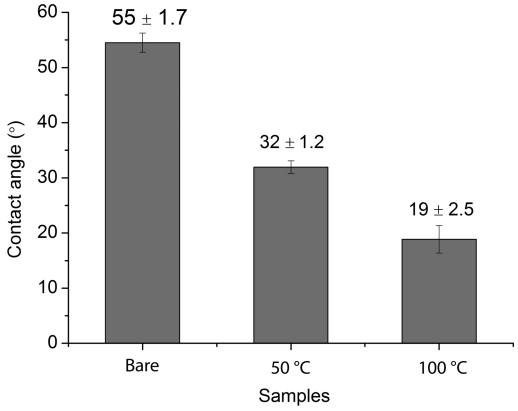

Figure 4. Static water contact angles of bare AZ31 and AZ31 samples IL treated at 50 and 100 °C.

angle of 55 ± 1.7°. IL treatment decreased the contact angle and thus increased the hydrophilicity of the surface. The surface after the IL treatment at 100 °C for 1 h was clearly more hydrophilic, with a much lower water contact angle of 19 ± 2.5°.

3.2. Immersion Behavior of $P_{1,4,4,4}$dpp IL Films in SBF. Figure 5 compares the corrosion morphologies of the AZ31

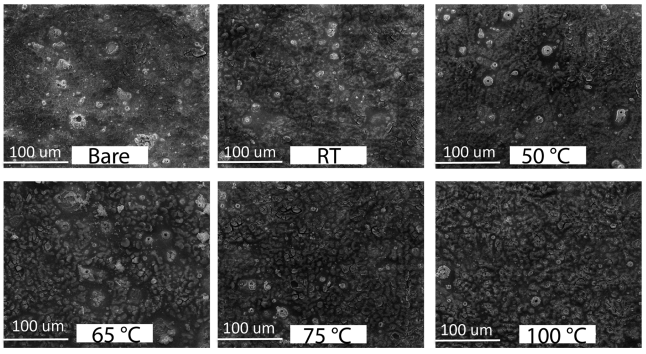

Figure 5. Typical SEM observations of AZ31 alloy surfaces after 2 h of immersion in 100 mL SBF at 37 °C. These alloys are bare control and after 1 h IL treatments at RT and at 50, 65, 75, or 100 °C.

samples after immersion in 100 mL SBF at 37 °C for 2 h, for a bare surface, and for five surfaces treated in $P_{1,4,4,4}$dpp IL at different treatment temperatures. As shown in Figure 5, for bare AZ31, the surface after immersion consisted of a background film with a cracked appearance together with a number of white, hemispherical caps. The background film was the corrosion product resulting from uniform corrosion, and its cracked appearance was probably caused by drying in the vacuum chamber of the SEM. These caps indicate localized pitting corrosion. The surfaces of the IL-treated samples after immersion appeared much cleaner than the bare sample surface, and there were fewer white caps on the surfaces of these IL-treated samples. Among the samples in Figure 5, the

sample that was treated at 100 °C had the fewest white caps on its surface. These observations suggest that IL treatment made corrosion occur more uniformly, and the surfaces after IL treatment were less sensitive to localized pitting corrosion.

To evaluate the corrosion morphology in more detail, we removed the corrosion products from the surfaces of some samples (bare and IL-treated at 50 and 100 °C). These surfaces were then examined using optical profilometry. Figure 6a shows

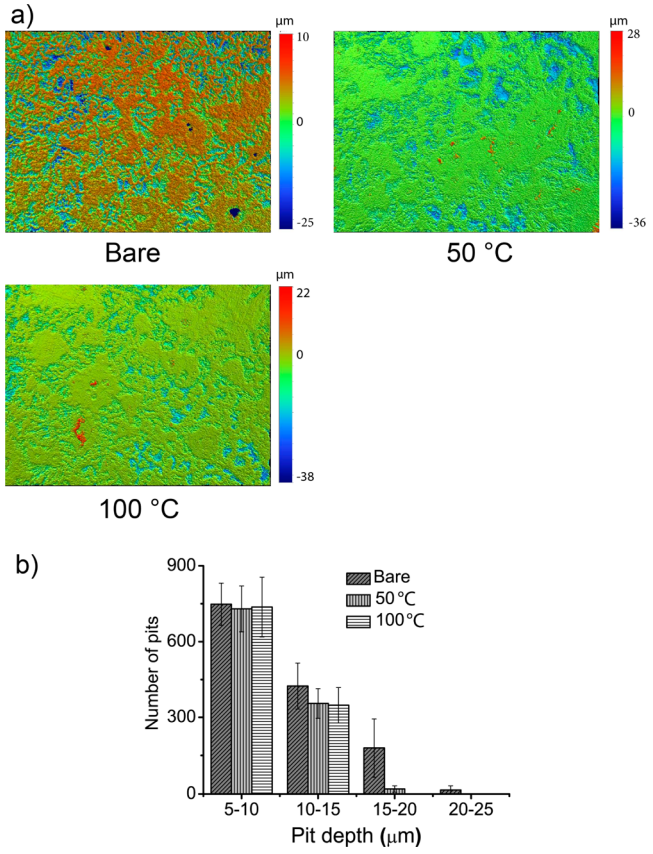

Figure 6. (a) Typical optical profilometry observations of surfaces after the removal of corrosion products from bare AZ31 and from AZ31 treated with IL at 50 and 100 °C. (b) Histogram of pit numbers at each pit depth for these samples.

typical three-dimensional surface images of these samples. In Figure 6, the surface of bare AZ31 appeared to be heavily attacked with some portions of the surface corroded away. For the AZ31 IL treated at 50 °C, while a few localized and large pits could still be observed, some parts of the surface appeared to be less corroded than the bare AZ31. In comparison, the surface of AZ31 IL treated at 100 °C had a distinctly different morphology from that of the other two samples. There were a number of shallow pits observed over the whole surface.

For more quantitative comparison of the corrosion severity, we determined the pit depths and the number of pits at each pit depth using optical profilometry over a 937.5 × 1250.0 μm field, as shown in Figure 6b. In the measurements, the size of all pits analyzed was limited to a pit mouth area of 10 μm^2. In this histogram, the effect of IL treatment is readily seen, with a dramatic decrease in the depth of pits. On the surface of bare AZ31, the range of pit depths extended to 25 μm. For the IL-treated samples, pits deeper than ~15 μm were effectively reduced. (e.g., if we consider pits in the 15−20 μm size range, there were ~10−20 pits/mm^2 on the surface of the AZ31 IL treated at 50 °C, ~1−2 pits/mm^2 on the surface of the AZ31 IL treated at 100 °C; this is a significant reduction compared to the bare AZ31 which had ~200 pits/mm^2).

3.3. Using EIS as a Diagnostic Tool for Comparing Corrosion Behavior. EIS was another approach used to evaluate the corrosion performance of these AZ31 samples in SBF. Each Nyquist plot could give an insight into the chemical reactions occurring at the interfaces between the samples and the solution at that time. In this study, EIS measurements were conducted at 10 min intervals for 2.5 h during exposure of surfaces to the SBF solution. Figure 7 shows a typical example

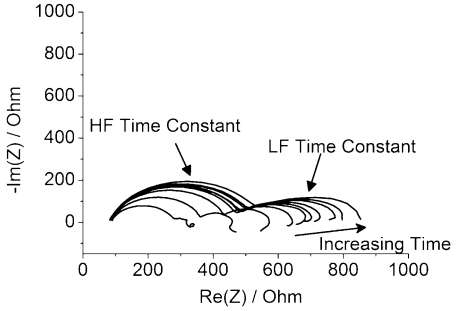

Figure 7. Typical Nyquist plots of impedance spectra obtained during immersion of IL-treated AZ31 in SBF. IL treatment was conducted at 100 °C.

of the evolution of Nyquist impedance spectra as a function of the immersion time for an AZ31 sample IL treated at 100 °C in $P_{1,4,4,4}$dpp IL. Bare AZ31 and other AZ31 samples that were treated with IL at various temperatures were also observed to exhibit similar behavior. The spectra followed the typical trends observed for Mg alloys of a double semicircle. The high frequency (HF) semicircles (to the left of the figure) were from the surface film, and the low frequency (LF) semicircles were from the charge transfer reaction in parallel with the double layer capacitance.[20] It was observed that both HF and LF semicircles increased in size with immersion time. During immersion, there was a gradual buildup of calcium apatite-like corrosion product on the surface. The accumulation of these corrosion products could increase both the surface film resistance and polarization resistance.[20] Thus, both HF and LF semicircles in the Nyquist plots were observed to increase in size with immersion time. The evolution of these Nyquist plots thereby reflects the evolution of the corrosion process of Mg alloys in the solution with immersion time.

The corrosion performance of bare AZ31 in SBF was compared with that of AZ31 that had been treated with IL at different temperatures, in Figure 8. The spectra were compared at two time points: at the beginning of immersion (t = 0 h), and after 2.5 h of immersion (t = 2.5 h). At t = 0 h (Figure 8a), there was a negligible amount of corrosion product deposited on the sample surface. The EIS spectra obtained at this point in time represented the surface films of these samples, that is, the $MgO/Mg(OH)_2$ for bare AZ31 and IL film for the IL-treated AZ31 samples.

After 2.5 h of immersion in SBF (Figure 8b), among the samples tested, the EIS spectrum for bare AZ31 had the largest semicircles, and the EIS spectrum for the AZ31 IL treated at 100 °C had the smallest semicircles. It was also observed that the size of the semicircles in these EIS spectra decreased with increasing treatment temperature. At this time, a layer of

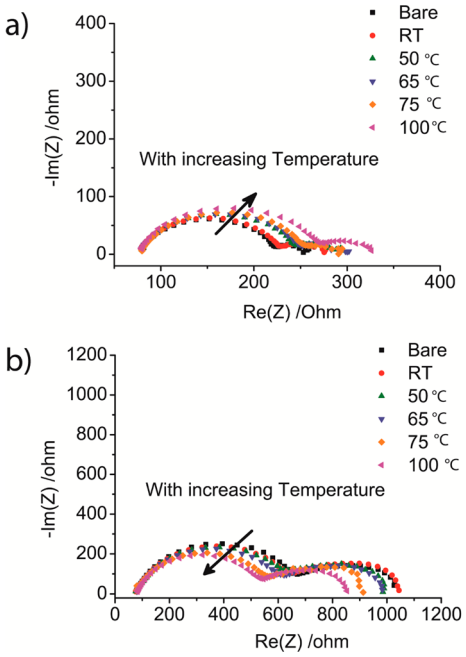

Figure 8. Comparison of the Nyquist plots at (a) t = 0 h and (b) t = 2.5 h acquired during immersion of samples in SBF. Samples are bare AZ31 and AZ31 IL treated for 1 h at RT and at 50, 65, 75, or 100 °C.

calcium-apatite like corrosion product was likely present on the sample surface. The thickness of this corrosion product layer was proportional to the size of the semicircles seen in the EIS spectrum. Given the smallest semicircles were seen in the EIS spectrum of the AZ31 IL-treated at 100 °C, it is logical to presume that this sample had the least deposition of corrosion products on the surface, indicating the slowest corrosion rate during the immersion process.

In Figure 9, the EIS spectra were fitted (using EC-Lab software) with a simplified equivalent circuit, for a quantitative comparison. The circuit consists of an electrolyte resistance, R_e, and two RC units in series, representing the double layer (R_t and C_{dl}) and the surface film (R_f and Q_f). An example of a fit is shown in Figure 9b. The surface film resistances were extracted by fitting this equivalent circuit to the HF arcs. The variation in the surface film resistances with respect to immersion time is shown in Figure 9c. The sample with best corrosion performance when exposed to the SBF is expected to have the highest initial surface film resistance at the beginning of immersion, which will increase at the slowest rate with immersion time and have the least increase for this film resistance with time in the SBF. It is obvious the AZ31 IL treated at 100 °C showed this behavior and therefore could be classified as having the best corrosion performance (with respect to rate of corrosion) out of the samples examined. Moreover, after 2.5 h of immersion, the rate of increase of surface film resistance for the two higher temperature treatments (50 and 100 °C) seemed to reach a shallow plateau, also indicating that the rate of corrosion has further decreased. This was in contrast with the other samples where the rate of increase of the surface film resistance was still high.

To better understand the effect of treatment temperatures on the distribution of IL films, Figure 10 highlights a parameter—the double layer capacitance (C_{dl}), extracted from fitting of the circuit to the first EIS loops obtained at the beginning of immersion. The double layer capacitance is related to the

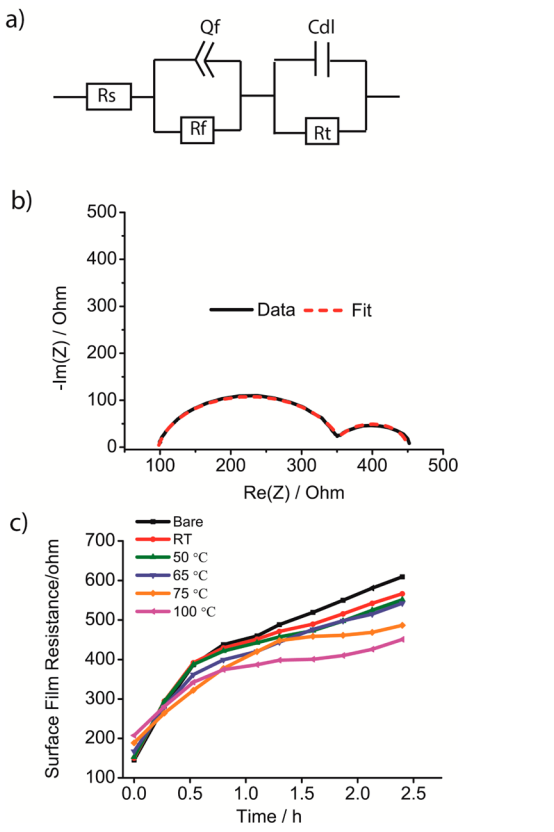

Figure 9. (a) Simplified equivalent circuit used to fit EIS data. R_s, R_f, R_t, C_{dl}, and Q_f are the solution resistance, film resistance, charge-transfer resistance, double layer capacitance, and constant phase element corresponding to the film, respectively. (b) Typical example showing experimental and fitted EIS data. (c) Change in surface film resistance (R_f) as a function of immersion time.

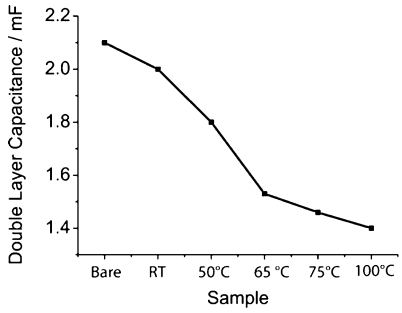

Figure 10. Surface film resistance (R_f) and double layer capacitance (Q_f), extracted from the higher-frequency part of the EIS spectrum measured immediately upon immersion in SBF, for the bare AZ31 and AZ31 IL-treated for 1 h at RT and at 50, 65, 75, and 100 °C.

physical properties of the surface and the electrolytes by the following equation: $C_{dl} = (\varepsilon\varepsilon_o A)/t$, where ε is the dielectric constant of the electrolyte, ε_o is 8.85 × 10^{-14} Farads/cm, A is the area, and t is thickness of the double layer. In this study, as these samples were immersed in the same SBF solution, the ε and t for the C_{dl} of these samples were the same, and thus, the C_{dl} was mainly area dependent. In this work, the 100 °C IL treatment produced the lowest C_{dl} of all the samples, which indicated that it has the smallest effective surface area exposed to the SBF, and therefore the largest area of AZ31 surface covered by IL film (or a much smoother/less rough surface).

dx.doi.org/10.1021/am506825d | ACS Appl. Mater. Interfaces 2014, 6, 18989−18997

3.4. Formation Mechanisms of $P_{1,4,4,4,}$dpp IL Film on AZ31 Surface. In the above discussion, we have shown that it is possible to develop a surface film using the low toxicity IL $P_{1,4,4,4}$dpp to enhance both the corrosion resistance and biocompatibility of Mg alloy AZ31 (in particular at the initial stage of implantation) for stent applications. The results also show that increasing treatment temperature was an effective approach to forming a more efficient IL film on the surface of AZ31. In this section, we discuss the interaction mechanisms between the IL and AZ31, which provide important chemical insight into the IL film formation process.

As shown above, ATR-FTIR spectra evidently indicate the existence of both cation and anion in the IL film, as well as the occurrence of chemical interactions between the dpp^- anion and the AZ31 surface in the treatment. The formation of an IL film on the surface of Mg alloy is a complicated process.[14,32] There are two possible mechanisms by which the dpp^- anion of the IL can interact with the metallic surface, discussed as follows.

As suggested by the ATR-FTIR characterization, the phenyl groups may be absent from the treated surface. This suggests the possibility that the dpp^- anions have undergone a chemical breakdown during the IL treatment process. If this were the case, previous investigations relating to the interaction between IL $P_{6,6,6,14}$dpp and Mg alloy ZE41 suggests that dpp^- anions in the ILs possibly undergo an electrochemical reduction reaction prior to surface film formation and that the phenyl group is cleaved, while the phosphate group itself is maintained.[14] Thus, it is possible that the dpp^- anions in this work undergo a similar reaction. It is also known that this attack on the phenyl-phosphate ester molecule usually occurs more readily under alkaline conditions on the surface.[33] With this understanding, one can envisage that during the treatment a certain amount of water from the atmosphere will be absorbed into the $P_{1,4,4,4}$dpp IL. When the water comes into contact with the AZ31 surface, the corrosion process of the AZ31 can lead to the release of Mg^{2+} and the formation of hydroxyl anions (OH^-). The accumulation of OH^- on the surface will increase local pH and thus catalyze the decomposition process of the anions in the IL. The ATR-FTIR data shows that in the IL film formation process, the anions chemically interact with AZ31 metal substrate to form a metal ester $[Mg{-}O{-}PO_2]^-$ on the surface. Because it has been shown by Forsyth et al. through NMR studies that the dpp IL can only interact strongly with a Mg alloy if it contains hydroxide groups on the surface,[34] it is assumed that the anions will undergo chemical reduction reactions with the O−H groups on the surface to form metal esters $[Mg{-}O{-}PO_2]^-$ and release H_2O molecules. With these considerations, the following reactions (Scheme 1) would theoretically define the IL film formation process.

On the other hand, there is a possibility that some of the dpp^- anions do not undergo the extensive decomposition process during the treatment and that the vibrations associated with the phenyl rings were absent from the ATR-FTIR for other reasons related to surface interactions. In this context, the Mg^{2+} ions formed by the corrosion of AZ31, will interact with dpp^- anions or with dpp^- anions and OH^- ions and form $Mg(dpp)_2$ or Mg(dpp)(OH), respectively, as shown in Scheme 2.

The $P_{1,4,4,4}$+ cations in the IL were found to be principally unaffected during the treatment. It is possible that these cations possibly electrostatically adsorb to the top of dpp^- anions to conserve charge neutrality, or both cations and anions electrostatically adsorb onto the sample surface.

Scheme 1. Possible Chemical Reactions of the dpp^- Anion with the AZ31 Surface Proposed to Explain the IL Film Formation Process

(1) $Mg = Mg^{2+} + 2e^-$

(2) $2H_2O + 2e^- = H_2 + 2OH^-$

(3) $Mg^{2+} + 2OH^- = Mg(OH)_2$

(4) $[(PhO)_2PO_2]^- + 2OH^- = [(OH)_2PO_2]^- + 2PhO^-$

(5) $[(HO)_2PO_2]^- + Mg(OH)_2 = Mg\text{-}O\text{-}PO_2^- + 2H_2O$

Scheme 2. Other Possible Chemical Reactions of the dpp^- Anion with the AZ31 Surface Proposed to Explain the Formation of the IL Film

$Mg^{2+} + 2dpp^- = Mg(dpp)_2$

$Mg^{2+} + dpp^- + OH^- = Mg(dpp)(OH)$

3.5. Effect of Treatment Temperature on the IL Film Formation and Its Corrosion Performance. The results have shown that the effect of treatment temperature on the formation of IL film on AZ31 is quite dramatic. The IL film formed at an elevated temperature was thicker and more hydrophilic and had a larger coverage area on the sample surface. In the previous studies related to the IL $P_{6,6,6,14}$dpp, it was found that when the IL reacted with Mg alloy ZE41, the reaction products are built up preferentially around intermetallic particles.[14] Thus, the effect of treatment temperature on the formation of IL film on the AZ31 surface is speculated as follows. At a lower treatment temperature condition (50 °C), the IL film deposits heterogeneously, mainly adjacent to some of the grain boundary phases. An elevated treatment temperature (100 °C) generates a more homogeneous and thicker IL film; in other words, there is more IL film deposited around most of the grain boundary phases compared to the sample treated at 50 °C + 1 h treatment condition. The reason for this effect can be related to the reaction rate. The rate of the chemical reactions occurring during the IL treatment process is accelerated by a higher treatment temperature, which leads to more IL reaction products deposited on the surface.

The immersion tests and EIS results show that the IL film is able to restrain the deposition of corrosion products on the surface and effectively suppress the pitting corrosion. For the bare AZ31, because its native passive $MgO/Mg(OH)_2$ surface film is unable to provide satisfactory corrosion protection to the underlying metal in SBF, upon exposure of the substrate to the solution, corrosion starts to occur quickly over the whole surface. With increasing immersion time, severe localized pitting corrosion occurs mostly adjacent to the intermetallic particles on the surface due to the galvanic potential dthoseifference between these intermetallic particles and the Mg matrix. The IL film is deposited preferentially around intermetallic particles during the IL treatment, which makes the regions near the intermetallic particles less prone to corrosion attack in the solution. Therefore, the IL treated surfaces are less sensitive to localized pitting corrosion in SBF. Among these samples, the IL surface film formed at 100 °C was thickest and

had the largest coverage area on the sample surface, which thereby led to the least number of pits on the sample surface.

It appears that the $P_{1,4,4,4}$dpp IL films (especially those formed at 100 °C treatment condition) show attractive features that result in a suitable surface film for biodegradable Mg stents. First, this film can suppress the formation of localized pitting corrosion on the surface, which is vital to avoid the early failure of biomedical implants through localized loss of the mechanical integrity. Second, the hydrophilic nature of this IL film on the surface can reduce the driving force for protein adsorption and the capacity for cell adhesion and thus improve the biocompatibility of stents in the body.[35,36] Lastly but not least, the IL treatment procedure is simple and easy to apply to the complex surface shapes associated with metallic cardiovascular stents, which is another reason for the extensive interest in IL-based surface treatments. Given all these characteristics, this simple chemical surface modification using $P_{1,4,4,4}$ dpp IL opens a possible new approach for coating biomedical Mg-based stents.

CONCLUSIONS

This work showed a systematic study to understand the effect of treatment temperature on producing an $P_{1,4,4,4}$dpp IL film on Mg alloy AZ31 with the ability to control corrosion degradation. The effectiveness and properties of these $P_{1,4,4,4}$dpp IL films formed on AZ31 Mg alloys at different treatment temperatures were evaluated by a combination of spectroscopic, microscopic, and electrochemical techniques. The results showed that increasing treatment temperature is capable of forming a more corrosion-resistive IL film, which can significantly reduce pitting corrosion. It was found that the IL film formed at a higher temperature was thicker and more hydrophilic and had a larger coverage area compared to the film formed at a lower temperature. Furthermore, this study utilized ATR-FTIR to get insight into the interaction mechanisms of the underlying the formation of $P_{1,4,4,4}$dpp IL film on Mg alloy. The IR spectra revealed a chemical reaction that formed a P−O−metal bond between the IL film and the AZ31 substrate, with both cation and anion present in the IL film. On the basis of the IR data, possible formation mechanisms for the IL film on the AZ31 surface were proposed. Moreover, it is proposed that at a lower treatment temperature, IL film deposited preferentially around some of the intermetallic phases. With increasing treatment temperature, there were more IL films deposited around most of intermetallic phases, and the IL film on the surface was more homogeneous. Therefore, there was less pitting corrosion observed on the AZ31 surface IL treated at a higher temperature. Clearly, treatment temperature plays an important role, and the temperature must be high enough to form a robust IL film. Of the tested samples, AZ31 treated by IL at 100 °C showed the best corrosion performance and surface hydrophilicity/biocompatibility. Such an anticorrosive and hydrophilic coating can be potentially applied to surfaces of Mg-based stents. Clearly, the next stage of this work requires confirmation of the biocompatibility of this coating on the Mg alloy. Our initial cytotoxicity tests for this IL (treated on stainless steel substrate) were undertaken on human coronary artery cells alone because a poorly protected Mg alloy surface itself leads to cell death for the generation of OH^- ions. Thus, a future objective will be to undertake the cytotoxicity test (or in vivo test) on an IL-coated sample with well-controlled degradation rate to avoid cell death encountered due to corrosion of Mg alone.

AUTHOR INFORMATION

Corresponding Author

*E-mail: maria.forsyth@deakin.edu.au. Tel: +61 392446727. Fax: +61 392446868.

Notes

The authors declare no competing financial interest.

ACKNOWLEDGMENTS

The authors would like to acknowledge Boston Scientific and the ARC for funding through the Centre of Excellence for Electromaterials Science (ACES) Linkage (project no. LP0990621). Acknowledgement is also given to Dr. Jiazeng Sun (Monash University) for preparing the IL; Dr. Jan Weber (Boston Scientific), Dr. Torsten Scheuermann (Boston Scientific), Prof. Gordon Wallace (The University of Wollongong), Dr. Simon Moulton (The University of Wollongong), and Dr. Kate Nairn (Monash University) for valuable comments.

REFERENCES

(1) Heublein, B.; Rohde, R.; Kaese, V.; Niemeyer, M.; Hartung, W.; Haverich, A. Biocorrosion of Magnesium Alloys: A New Principle in Cardiovascular Implant Technology? *Heart* **2003**, *89*, 651−656.

(2) Hermawan, H.; Dube, D.; Mantovani, D. Developments in Metallic Biodegradable Stents. *Acta Biomater.* **2010**, *6*, 1693−1697.

(3) Kirkland, N. T.; Birbilis, N.; Walker, J.; Woodfield, T.; Dias, G. J.; Staiger, M. P. In Vitro Dissolution of Magnesium-Calcium Binary Alloys: Clarifying the Unique Role of Calcium Additions in Bioresorbable Magnesium Implant Alloys. *J. Biomed. Mater. Res., Part B* **2010**, *95*, 91−100.

(4) Vormann, J. Magnesium: Nutrition and Metabolism. *Mol. Aspects Med.* **2003**, *24*, 27−37.

(5) Witte, F. The History of Biodegradable Magnesium Implants: A Review. *Acta Biomater.* **2010**, *6*, 1680−1692.

(6) Ghali, E.; Dietzel, W.; Kainer, K.-U. General and Localized Corrosion of Magnesium Alloys: A Critical Review. *J. Mater. Eng. Perform.* **2004**, *13*, 7−23.

(7) Staiger, M. P.; Pietak, A. M.; Huadmai, J.; Dias, G. Magnesium and Its Alloys as Orthopedic Biomaterials: A Review. *Biomaterials* **2006**, *27*, 1728−1734.

(8) Ye, S. H.; Jang, Y. S.; Yun, Y. H.; Shankarraman, V.; Woolley, J. R.; Hong, Y.; Gamble, L. J.; Ishihara, K.; Wagner, W. R. Surface Modification of a Biodegradable Magnesium Alloy with Phosphorylcholine (Pc) and Sulfobetaine (Sb) Functional Macromolecules for Reduced Thrombogenicity and Acute Corrosion Resistance. *Langmuir* **2013**, *29*, 8320−8327.

(9) Erbel, R.; Di Mario, C.; Bartunek, J.; Bonnier, J.; de Bruyne, B.; Eberli, F. R.; Erne, P.; Haude, M.; Heublein, B.; Horrigan, M.; Ilsley, C.; Bose, D.; Koolen, J.; Luscher, T. F.; Weissman, N.; Waksman, R. Temporary Scaffolding of Coronary Arteries with Bioabsorbable Magnesium Stents: A Prospective, Non-Randomised Multicentre Trial. *Lancet* **2007**, *369*, 1869−1875.

(10) Chen, X. B.; Birbilis, N.; Abbott, T. B. Review of Corrosion-Resistant Conversion Coatings for Magnesium and Its Alloys. *Corrosion* **2011**, *67*, 035005-1−035005-16.

(11) Blawert, C.; Dietzel, W.; Ghali, E.; Song, G. Anodizing Treatments for Magnesium Alloys and Their Effect on Corrosion Resistance in Various Environments. *Adv. Eng. Mater.* **2006**, *8*, 511−533.

(12) Liu, X.; Yue, Z.; Romeo, T.; Weber, J.; Scheuermann, T.; Moulton, S.; Wallace, G. Biofunctionalized Anti-Corrosive Silane Coatings for Magnesium Alloys. *Acta Biomater.* **2013**, *9*, 8671−8677.

(13) Ostrowski, N. J.; Lee, B.; Roy, A.; Ramanathan, M.; Kumta, P. N. Biodegradable Poly(lactide-*co*-glycolide) Coatings on Magnesium Alloys for Orthopedic Applications. *J. Mater. Sci. Mater. Med.* **2013**, *24*, 85−96.

(14) Forsyth, M.; Neil, W. C.; Howlett, P. C.; MacFarlane, D. R.; Hinton, B. R. W.; Rocher, N.; Kemp, T. F.; Smith, M. E. New Insights into the Fundamental Chemical Nature of Ionic Liquid Film Formation on Magnesium Alloy Surfaces. *ACS Appl. Mater. Interfaces* **2009**, *1*, 1045−1052.
(15) Ohno, H., Importance and Possibility of Ionic Liquids. In *Electrochemical Aspects of Ionic Liquids*; Wiley: Hoboken, N.J., 2011; Chapter 1, pp 1−3.
(16) Ferraz, R.; Branco, L. C.; Prudencio, C.; Noronha, J. P.; Petrovski, Z. Ionic Liquids as Active Pharmaceutical Ingredients. *ChemMedChem.* **2011**, *6*, 975−985.
(17) Seter, M.; Thomson, M. J.; Stoimenovski, J.; MacFarlane, D. R.; Forsyth, M. Dual Active Ionic Liquids and Organic Salts for Inhibition of Microbially Influenced Corrosion. *Chem. Commun.* **2012**, *48*, 5983−5985.
(18) Fujita, K.; MacFarlane, D. R.; Forsyth, M. Protein Solubilising and Stabilising Ionic Liquids. *Chem. Commun.* **2005**, 4804−4806.
(19) Frade, R. F.; Afonso, C. A. Impact of Ionic Liquids in Environment and Humans: An Overview. *Hum. Exp. Toxicol.* **2010**, *29*, 1038−1054.
(20) Zhang, Y. F.; Hinton, B.; Wallace, G.; Liu, X.; Forsyth, M. On Corrosion Behaviour of Magnesium Alloy AZ31 in Simulated Body Fluids and Influence of Ionic Liquid Pretreatments. *Corros. Eng., Sci. Technol.* **2012**, *47*, 374−382.
(21) Howlett, P. C.; Tan; S. K.; Zhang, S.; Efthimiadis, J.; MacFarlane, D. R.; Forsyth, M. Novel Conversion Coatings for Magnesium Alloy AZ31 Using Ionic Liquids. In *Proceedings of the Australasian Corrosion Association (ACA) Corrosion and Protection Conference*, Hobart, Australia, Nov 19−22, 2006; Australasian Corrosion Association: Victoria, Australia, 2006; pp 475−480.
(22) Latham, J.-A.; Howlett, P. C.; MacFarlane, D. R.; Somers, A.; Forsyth, M. Anodising AZ31 in a Phosphonium Ionic Liquid: Corrosion Protection through Composite Film Deposition. *J. Electrochem. Soc.* **2012**, *159*, C539−C545.
(23) Xin, Y.; Huo, K.; Hu, T.; Tang, G.; Chu, P. K. Corrosion Products on Biomedical Magnesium Alloy Soaked in Simulated Body Fluids. *J. Mater. Res.* **2009**, *24*, 2711−2719.
(24) Rettig, R.; Virtanen, S. Composition of Corrosion Layers on a Magnesium Rare-Earth Alloy in Simulated Body Fluids. *J. Biomed. Mater. Res., Part A* **2009**, *88*, 359−369.
(25) Kokubo, T.; Takadama, H. How Useful Is SBF in Predicting in Vivo Bone Bioactivity? *Biomaterials* **2006**, *27*, 2907−2915.
(26) Witte, F.; Fischer, J.; Nellesen, J.; Crostack, H.-A.; Kaese, V.; Pisch, A.; Beckmann, F.; Windhagen, H. In Vitro and in Vivo Corrosion Measurements of Magnesium Alloys. *Biomaterials* **2006**, *27*, 1013−1018.
(27) Walker, J.; Shadanbaz, S.; Kirkland, N. T.; Stace, E.; Woodfield, T.; Staiger, M. P.; Dias, G. J. Magnesium Alloys: Predicting in Vivo Corrosion with in Vitro Immersion Testing. *J. Biomed. Mater. Res., Part B* **2012**, *100*, 1134−41.
(28) Witte, F.; Hort, N.; Vogt, C.; Cohen, S.; Kainer, K. U.; Willumeit, R.; Feyerabend, F. Degradable Biomaterials Based on Magnesium Corrosion. *Curr. Opin. Solid State Mater. Sci.* **2008**, *12*, 63−72.
(29) Xu, D. K.; Birbilis, N.; Lashansky, D.; Rometsch, P. A.; Muddle, B. C. Effect of Solution Treatment on the Corrosion Behaviour of Aluminium Alloy AA7150: Optimisation for Corrosion Resistance. *Corros. Sci.* **2011**, *53*, 217−225.
(30) Cavanaugh, M. K.; Buchheit, R. G.; Birbilis, N. Modeling the Environmental Dependence of Pit Growth Using Neural Network Approaches. *Corros. Sci.* **2010**, *52*, 3070−3077.
(31) Socrates, G. *Infrared and Raman Characteristic Group Frequencies: Tables and Charts*. 3rd ed.; Wiley: New York, 2004.
(32) Efthimiadis, J.; Neil, W. C.; Bunter, A.; Howlett, P. C.; Hinton, B. R.; MacFarlane, D. R.; Forsyth, M. Potentiostatic Control of Ionic Liquid Surface Film Formation on ZE41 Magnesium Alloy. *ACS Appl. Mater. Interfaces* **2010**, *2*, 1317−1323.
(33) O'Brien, P. J.; Herschlag, D. Alkaline Phosphatase Revisited: Hydrolysis of Alkyl Phosphates. *Biochemistry* **2002**, *41*, 3207−3225.
(34) Forsyth, M.; Kemp, T. F.; Howlett, P. C.; Sun, J.; Smith, M. E. A Potential Novel Rapid Screening NMR Approach to Boundary Film Formation at Solid Interfaces in Contact with Ionic Liquids. *J. Phys. Chem. C* **2008**, *112*, 13801−13804.
(35) Cunliffe, D.; Smart, C. A.; Alexander, C.; Vulfson, E. N. Bacterial Adhesion at Synthetic Surfaces. *Appl. Environ. Microbiol.* **1999**, *65*, 4995−5002.
(36) Vendra, V. K.; Wu, L.; Krishnan, S., Polymer Thin Films for Biomedical Applications. In *Nanotechnologies for the Life Sciences: Nanostructured Thin Films and Surfaces*; Kumar, C. S. S. R., Ed.; Wiley-VCH Verlag GmbH & Co. KGaA: Weinheim, 2007; Vol. 5.